

Energy band and charge-carrier engineering in skutterudite thermoelectric materials

Zhiyuan Liu(刘志愿), Ting Yang(杨婷), Yonggui Wang(王永贵), Ailin Xia(夏爱林), and Lianbo Ma(马连波)
Citation: Chin. Phys. B, 2022, 31 (**10**): 107303. DOI: 10.1088/1674-1056/ac6ee8
Journal homepage: http://cpb.iphy.ac.cn; http://iopscience.iop.org/cpb

What follows is a list of articles you may be interested in

Facile fabrication of highly flexible, porous PEDOT: PSS/SWCNTs films for thermoelectric applications

Fu-Wei Liu(刘福伟), Fei Zhong(钟飞), Shi-Chao Wang(王世超), Wen-He Xie(谢文合), Xue Chen(陈雪), Ya-Ge Hu(胡亚歌), Yu-Ying Ge(葛钰莹), Yuan Gao(郜源), Lei Wang(王雷), and Zi-Qi Liang(梁子骐)
Chin. Phys. B, 2022, 31 (**2**): 027303. DOI: 10.1088/1674-1056/ac3502

Enhanced thermoelectric properties in two-dimensional monolayer Si_2BN by adsorbing halogen atoms

Cheng-Wei Wu(吴成伟), Changqing Xiang(向长青), Hengyu Yang(杨恒玉), Wu-Xing Zhou(周五星), Guofeng Xie(谢国锋), Baoli Ou(欧宝立), and Dan Wu(伍丹)
Chin. Phys. B, 2021, 30 (**3**): 037304. DOI: 10.1088/1674-1056/abd163

Electronic and thermoelectric properties of alkali metal-based perovskites $CsYbF_3$ and $RbYbF_3$

Q Mahmood, N A Noor, T Ghrib, Nessrin A Kattan, Asif Mahmood, and Shahid M Ramay
Chin. Phys. B, 2020, 29 (**11**): 117305. DOI: 10.1088/1674-1056/ab9de3

Influence of spherical inclusions on effective thermoelectric properties of thermoelectric composite materials

Wen-Kai Yan(闫文凯), Ai-Bing Zhang(张爱兵), Li-Jun Yi(易利军), Bao-Lin Wang(王保林), Ji Wang(王骥)
Chin. Phys. B, 2020, 29 (**5**): 057301. DOI: 10.1088/1674-1056/ab7d96

Strategies for optimizing the thermoelectricity of PbTe alloys

Jinze Zhai(翟近泽), Teng Wang(王腾), Hongchao Wang(王洪超), Wenbin Su(苏文斌), Xue Wang(王雪), Tingting Chen(陈婷婷), Chunlei Wang(王春雷)
Chin. Phys. B, 2018, 27 (**4**): 047306. DOI: 10.1088/1674-1056/27/4/047306

REVIEW

Energy band and charge-carrier engineering in skutterudite thermoelectric materials

Zhiyuan Liu(刘志愿)[1,2,†], Ting Yang(杨婷)[2], Yonggui Wang(王永贵)[2], Ailin Xia(夏爱林)[1,2], and Lianbo Ma(马连波)[1,2]

[1] *Key Laboratory of Green Fabrication and Surface Technology of Advanced Metal Materials (Ministry of Education), Anhui University of Technology, Maanshan* 243002, *China*

[2] *School of Materials Science and Engineering, Anhui University of Technology, Maanshan* 243002, *China*

(Received 29 March 2022; revised manuscript received 2 May 2022; accepted manuscript online 12 May 2022)

The binary $CoSb_3$ skutterudite thermoelectric material has high thermal conductivity due to the covalent bond between Co and Sb, and the thermoelectric figure of merit, *ZT*, is very low. The thermal conductivity of $CoSb_3$ materials can be significantly reduced through phonon engineering, such as low-dimensional structure, the introduction of nano second phases, nanointerfaces or nanopores, which greatly improves their *ZT* values. The phonon engineering can optimize significantly the thermal transport properties of $CoSb_3$-based materials. However, the improvement of the electronic transport properties is not obvious, or even worse. Energy band and charge-carrier engineering can significantly improve the electronic transport properties of $CoSb_3$-based materials while optimizing the thermal transport properties. Therefore, the decoupling of thermal and electronic transport properties of $CoSb_3$-based materials can be realized by energy band and charge-carrier engineering. This review summarizes some methods of optimizing synergistically the electronic and thermal transport properties of $CoSb_3$ materials through the energy band and charge-carrier engineering strategies. Energy band engineering strategies include band convergence or resonant energy levels caused by doping/filling. The charge-carrier engineering strategy includes the optimization of carrier concentration and mobility caused by doping/filling, forming modulation doped structures or introducing nano second phase. These strategies are effective means to improve performance of thermoelectric materials and provide new research ideas of development of high-efficiency thermoelectric materials.

Keywords: $CoSb_3$-based skutterudite materials, energy band engineering, charge-carrier engineering, thermoelectric properties

PACS: 73.50.Lw, 84.60.Rb, 74.25.F–, 74.25.fc **DOI:** 10.1088/1674-1056/ac6ee8

1. Introduction

The development of environment-friendly renewable new energy and energy conversion technologies has attracted extensive attention of global researchers. Thermoelectric (TE) conversion is an environmentally friendly new energy conversion technology, which mainly uses the Seebeek, Peltier and Thomson effects of materials to realize mutual conversion of thermal and electronic energy. It has wide application prospects in the fields towards TE power generation recycling and TE refrigeration of dispersive heat sources, such as solar energy, industrial waste heat, and car exhaust waste heat.[1,2] TE properties exist in a kind of functional materials that use the movement of carriers inside to achieve mutual conversion of thermal and electrical energy. The comprehensive transport properties of TE materials can be characterized by the dimensionless TE figure of merit, i.e., *ZT*. $ZT = S^2\sigma T/\kappa$, where S is the Seebeck coefficient, σ is the electrical conductivity, κ is the thermal conductivity, and T is the absolute temperature. The κ is composed of electronic thermal conductivity (κ_E) and lattice thermal conductivity (κ_L). TE materials can be divided into low temperature (< 500 K), medium temperature (500–900 K) and high temperature (> 900 K) TE materials according to the service temperature.

Among many medium-temperature TE materials,[3–10] skutterudite[11–20] is one of the most promising TE materials. The binary $CoSb_3$ skutterudite TE material has high thermal conductivity and low *ZT* value due to the covalent bonding between the framework atoms.[21] Phonon engineering such as low dimensionalization,[22–24] the introduction of nano second phase,[25–28] nanointerfaces or nanopores,[29–31] phonon resonance scattering induced by filler[17,32,33] has been adopted to reduce remarkably the thermal conductivity of $CoSb_3$ materials, which significantly improves their *ZT* values. Although the thermal conductivity can be significantly reduced by adjusting the microstructure of the $CoSb_3$ material at the nanomesoscopic scale, it is also accompanied by deterioration of electrical conductivity of the material. As a result, the room for improving the electronic transport properties of $CoSb_3$ materials is limited. Therefore, it is particularly critical to explore methods that can not only optimize the thermal transport performance of $CoSb_3$ materials, but also improve the electronic transport performance. In recent years, some energy band engineering[34–41] and charge-carrier engineering opti-

[†]Corresponding author. E-mail: zhiyuanliu826@ahut.edu.cn

© 2022 Chinese Physical Society and IOP Publishing Ltd

mization strategies[42–44] have been proposed. Band engineering strategies mainly include band convergence and resonance energy levels. Charge-carrier engineering strategies mainly include the optimization and improvement of carrier concentration and mobility. These strategies are effective means to improve the electronic transport performance of TE materials, and provide new research ideas of the development of high-efficiency TE materials, which also provide a valuable reference for improvement of properties of $CoSb_3$-based skutterudite TE materials.

This review mainly summarizes some methods to optimize the electronic transport properties of $CoSb_3$ materials through energy band and charge-carrier engineering, as shown in Fig. 1. These methods mainly include: (1) band engineering strategies of band convergence and resonance levels induced by doping/filling foreign elements, (2) charge-carrier engineering strategies of carrier concentration or mobility enhancement caused by alloying, element filling and the introduction of nano second phase or special structure. These optimization methods have greatly improved the TE properties of $CoSb_3$-based skutterudite materials.

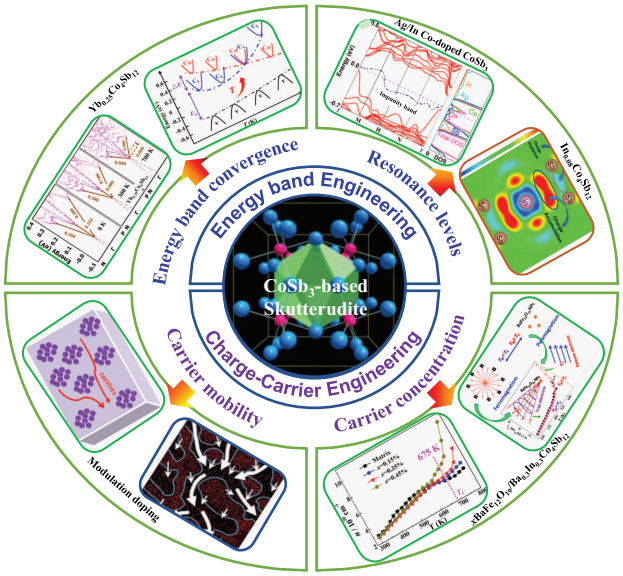


Fig. 1. Energy band and charge-carrier engineering in $CoSb_3$-based skutterudite TE materials. Reproduced with permission from Refs. [25, 45–49].

2. Energy band engineering

In recent years, applications of energy band engineering in TE materials have achieved fruitful results.[34–41] Solid solution alloys are formed by doping appropriate elements into the materials. The energy band structure of solid solution alloys will mainly show the following two changes: (i) Energy band degeneracy is improved. The multi-energy valley band degeneracy N_v is related to the total density of states (DOS) effective mass m_d^* and the single band DOS effective mass m_b^*, as shown in Eq. (1).[36,50] The increase in N_v can cause the increase of m_d^*. Then, Seebeck coefficient of the material can be significantly improved, as shown in Eq. (2).[51]

$$m_d^* = N_v^{2/3} m_b^*, \tag{1}$$

$$S = \left(8\pi^2 k_B^2 / 3eh^2\right) m_d^* T \left(\pi/3n\right)^{2/3} (r+1), \tag{2}$$

where k_B is Boltzmann's constant, h is Planck's constant, n is the carrier concentration, and r is the scattering factor. (ii) Resonant energy levels are generated.[52–54] Resonant levels will appear when the energy levels produced by the doped atom are located in the conduction band or valence band of a semiconductor matrix material. Its appearance will distort the density of states, cause narrow peaks in the density of states, and affect the transport of electrons, resulting in resonance scattering. In addition, the resonance energy level itself is a delocalized energy level with band conduction.[55] These factors affect significantly the Seebeck coefficient of the material. For $CoSb_3$-based skutterudite TE materials, these changes of energy band structure caused by doping/filling will lead to significant increase of Seebeck coefficient. Combined with the strong phonon scattering induced by doping/filling, the decoupling of thermal and electronic transport parameters is realized, which greatly improves the TE properties of $CoSb_3$-based materials.[56–65] Table 1 lists the optimized Seebeck coefficient and ZT values of some typical $CoSb_3$-based skutterudite TE materials[46,47,56–59,62–65] reported in recent years by the energy band engineering.

Table 1. The Seebeck coefficient and ZT values of some typical $CoSb_3$-based skutterudite TE materials optimized by the energy band engineering in recent years.

n-type skutterudite	$\lvert S\rvert_{max}$ ($\mu V \cdot K^{-1}$)	ZT_{max}	Ref.
Ag/In co-doped $CoSb_3$ (thin film)	200	0.65	[46]
$In_{0.08}Co_4Sb_{12}$	259	–	[47]
$In_{.26}Co_4Sb_{12}$	240	1.0	[56]
$In_{0.27}Co_4Sb_{11.9}$	230	1.2	[57]
$S_{0.125}Co_{3.5}Pt_{0.5}Sb_{12}$	204	–	[58]
$Yb_xCo_4Sb_{12}$	100	1.2	[59]
$Yb_yGa_{0.15}Co_4Sb_{11.95}$	250	1.25	[62]
$Yb_{0.3}Ca_{0.1}Al_{0.1}Ga_{0.1}In_{0.1}Co_{3.75}Fe_{0.25}Sb_{12}$	222	1.7	[63]
$Ga_{0.087}Co_4Sb_{12}$	28	0.7	[64]
$Ni_{0.07}Co_{0.93}Sb_{2.94}Te_{0.06}$	175	0.9	[65]

2.1. Energy band convergence

Energy band convergence is a method to reduce the energy difference between light and heavy bands (valence band or conduction band) through element doping. After effective element doping/filling, the energy gap between the light and heavy energy bands becomes smaller, so that the heavy bands can participate more in the transport of carriers and improve the energy valley degeneracy N_v, which leads to a significant improvement in the electronic transport properties of the material.

In recent years, energy band convergence has also been applied to $CoSb_3$-based materials,[56–65] which has greatly improved their thermoelectric properties. Tang *et al.*[59] proved that the first conduction band and the high-energy second

conduction band of the $CoSb_3$ and doped samples (such as Yb-filled skutterudite) were degenerated at high temperatures through theoretical calculation and experimental investigation. This is mainly due to the gradual decrease of the band gap between the first/secondconduction bands (CB1/CB2) and the valence band with increasing temperature. This result is consistent with the theoretical research results of Wang *et al.*[45] and Hanus *et al.*,[60] as shown in Fig. 2. The convergence of two conduction bands (CB1 and CB2) combined with valence band realizes the formation of three-band mode. More carriers participate in the electronic transport, which realizes the improvement of high-temperature electrical performance of the $Yb_{0.25}Co_4Sb_{12}$ material. The Fermi surface moves to the conduction band (Fig. 2(d)) by Yb doping. In convergence of the three-band mode and high-temperature double conduction band, more carriers are involved in the transport. The high-temperature performance of the $Yb_xCo_4Sb_{12}$ material is significantly improved. A high *ZT* value of 1.2 was obtained at 800 K.[59] Shi *et al.*[61] prepared a high-performance $Yb_xGa_yCo_4Sb_{12-y/3}$ sample in which Ga element replaced Sb in $Yb_xCo_4Sb_{12}$ skutterudite and occupied icosahedral voids at the same time (Fig. 3(a)). The first-principles calculation results show that double occupancy of Ga element destroys the symmetry of the frame Sb–Sb network, splits the deep triple degenerate conduction bands, and drives them down to the band edge, as shown in Fig. 3(b). The charge-compensation feature of the double occupancy of Ga element increases the total fill fraction limit. The Fermi level is raised to the extent that the carrier is close to these features in energy by giving this unique band structure feature and increasing the Yb filling content. The participation of these heavier energy bands in electron transport increases the Seebeck coefficient and carrier effective mass. In addition, the localized distortion caused by the Ga/Sb substitution enhances phonon scattering and effectively reduces the lattice thermal conductivity [Fig. 3(c)]. The highest *ZT* value of the $Yb_xGa_yCo_4Sb_{12-y/3}$ sample reached 1.25 at 780 K [Fig. 3(d)]. Zhang *et al.*[62] synthesized a $Co_{3.75}Fe_{0.25}Sb_{12}$ skutterudite TE material filled with five elements of Yb, Al, Ga, In, and Ca by using the melting spinning combined with SPS sintering technology (MS-SPS) (Fig. 4(a)). Five elements are filled into the icosahedral nanvoids of skutterudite, resulting in the comparable energy of multiple energy bands at Γ and *H* points and the convergence of energy bands (Figs. 4(c)–4(d)). Effective band convergence increases the electronic density of states of the multi-filled skutterudite near the Fermi level, resulting in the increase of the Seebeck coefficient. Specifically, the Seebeck coefficient of the multi-filled $Yb_{0.3}Ca_{0.1}Al_{0.1}Ga_{0.1}In_{0.1}Co_{3.75}Fe_{0.25}Sb_{12}$ sample is higher than that of the $Yb_{0.35}Co_{3.75}Fe_{0.25}Sb_{12}$ sample at similar carrier concentrations, as shown in Fig. 4(b). At the same time, the microstructure shows that more nanoparticles, dislocations, and lattice strain fields are formed in multi-filled skutterudite material (Fig. 4(a)). These microstructures can strongly scatter broadband phonons, resulting in a significant reduction in lattice thermal conductivity of the material. As a result, the *ZT* value of the five elements-filled skutterudite material reached 1.7 at 823 K. Therefore, it is a very effective means to improve the TE properties of $CoSb_3$-based materials by the energy band convergence induced by doping/filling.

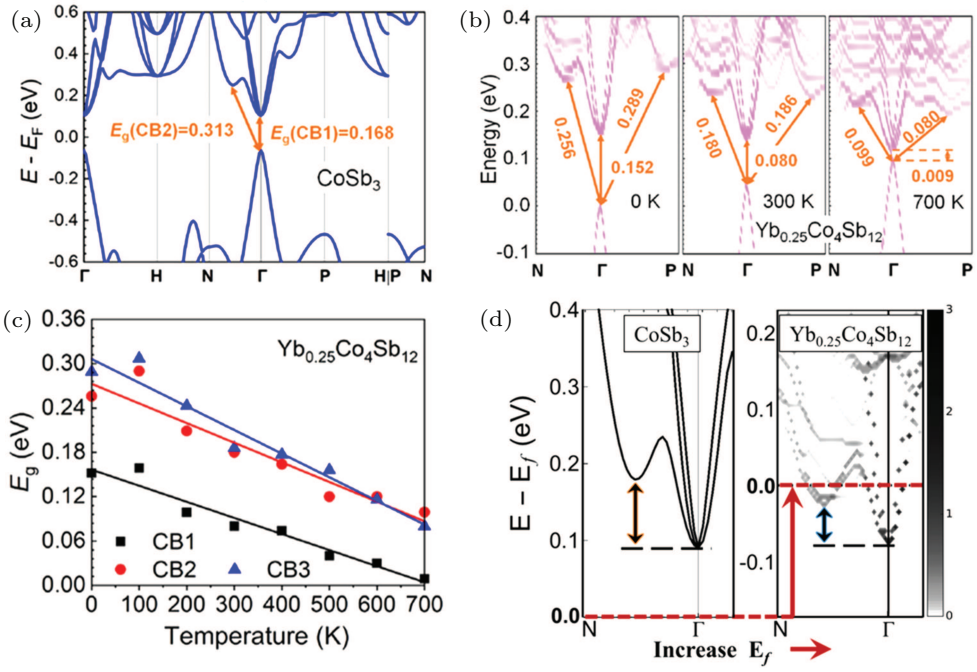


Fig. 2. (a) Band structure of the $CoSb_3$; (b) band structures of $Yb_{0.25}Co_4Sb_{12}$ sample at 0 K, 300 K and 700 K; (c) band gaps as functions of temperature for $Yb_{0.25}Co_4Sb_{12}$ sample. Reproduced with permission from Ref. [45]. (d) Band structures of the $CoSb_3$ and $Yb_{0.25}Co_4Sb_{12}$ samples. Reproduced with permission from Ref. [60].

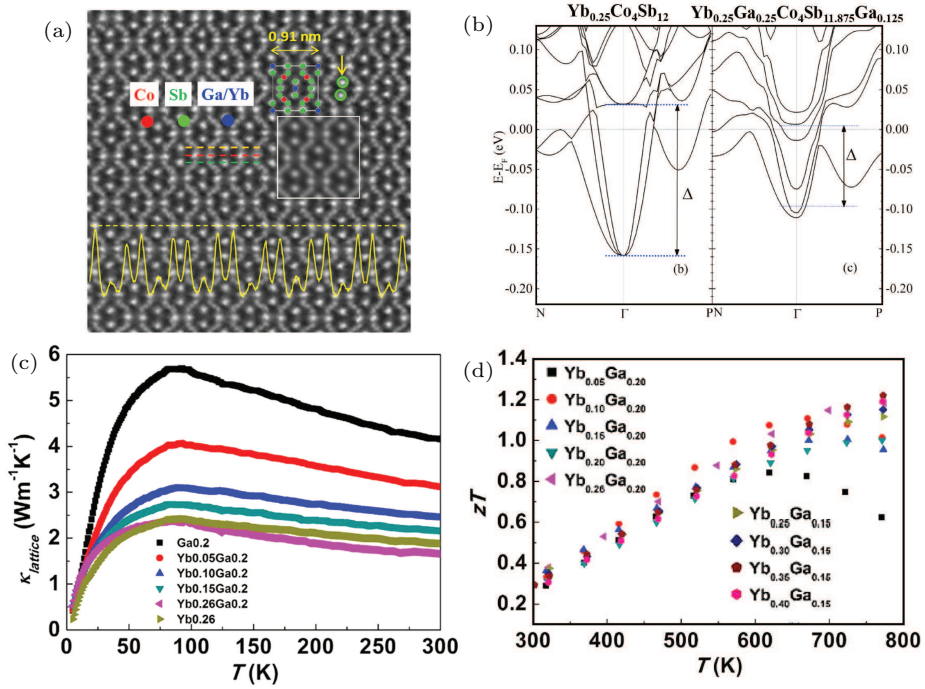


Fig. 3. (a) Scanning transmission electron microscope-high angle annular dark field (STEM-HAADF) image of $Yb_xGa_yCo_4Sb_{12-y/3}$ sample; (b) first-principles band structure calculation of $Yb_{0.25}Co_4Sb_{12}$ and $Yb_{0.25}Ga_{0.25}Co_4Sb_{11.875}Ga_{0.125}$ samples; (c) lattice thermal conductivity of $Yb_xGa_{0.2}Co_4Sb_{11.9333}$ ($x = 0$, 0.05, 0.10, 0.15, 0.26) and $Yb_{0.26}Co_4Sb_{12}$; (d) ZT value of $Yb_xGa_yCo_4Sb_{12-y/3}$ samples with different Yb and Ga concentrations. Reproduced with permission from Ref. [61].

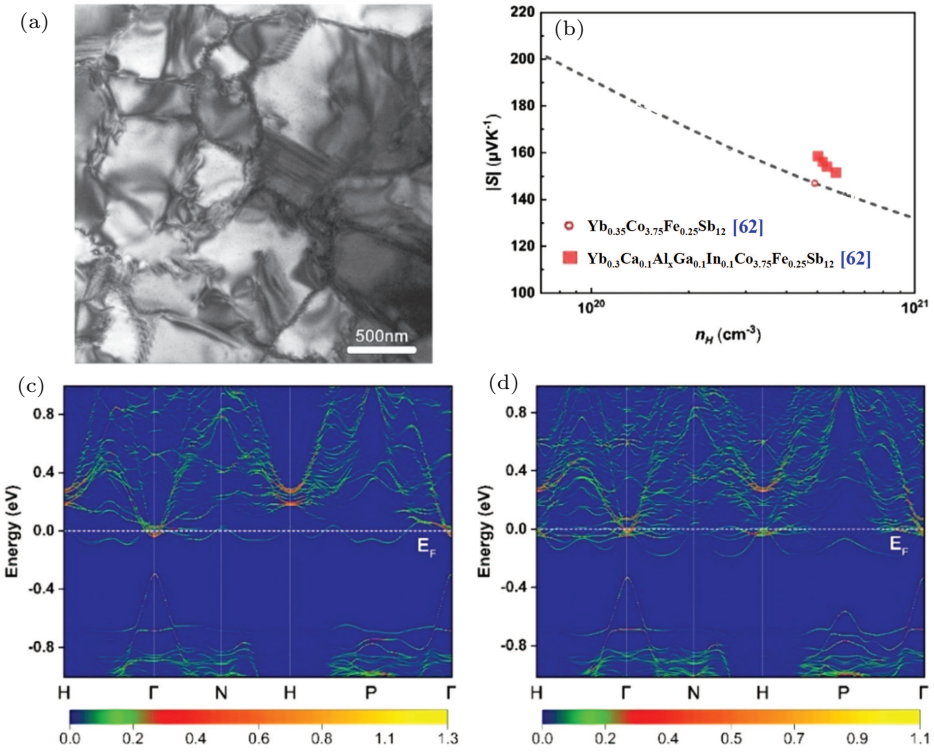


Fig. 4. (a) TEM image of the $Yb_{0.3}Ca_{0.1}Al_{0.1}Ga_{0.1}In_{0.1}Co_{3.75}Fe_{0.25}Sb_{12}$ sample; (b) the relationship between the Seebeck coefficient and the carrier concentration (n_H) of the $Yb_{0.3}Ca_{0.1}Al_xGa_{0.1}In_{0.1}Co_{3.75}Fe_{0.25}Sb_{12}$ sample. Band structure of (c) $Yb_{0.25}Co_{3.75}Fe_{0.25}Sb_{12}$ and (d) $Yb_{0.25}Al_{0.125}Ga_{0.125}In_{0.125}Co_{3.75}Fe_{0.25}Sb_{12}$. Reproduced with permission from Ref. [62].

2.2. Resonance levels

Resonance levels refer to the introduction of impurity levels in the matrix material through element doping/filling. The introduction of impurity levels can cause local "convexity" in the density of states $g(E)$ near the Fermi level E_F, as shown in Fig. 5. That is to say, the introduction of impurity atoms causes the resonance energy level (impurity state) in the conduction band or valence band of the TE matrix material, resulting in the distortion of the density of states near the Fermi level and the narrow peaks (convexity) in the density of states, which

ultimately affects electron transport. According to the following Mott formula,[66] the Seebeck coefficient is proportional to the density of states near the Fermi level. The steeper the density-of-states curve, the greater the slope, and the greater the Seebeck coefficient. The Seebeck coefficient $S(n)$ can be maximized under a given carrier concentration n, thereby maximizing the power factor $S^2\sigma$.[51]

$$S = \frac{\pi}{3}\frac{k_B}{e}(k_B T)\left\{\frac{\mathrm{d}\left[\ln\left(\sigma(E)\right)\right]}{\mathrm{d}E}\right\}, \tag{3}$$

$$\sigma(E) = \int \frac{e^2 L^2}{\tau k_B T} f(1-f) N(E)\,\mathrm{d}E, \tag{4}$$

where $N(E)$ is the density of states; $\sigma(E)$ is the differential electrical conductivity, which is used to describe the contribution of electrons with energy E to the overall electrical conductivity, as a function of the Fermi level; τ is the scattering time; L is the scattering distance (mean free path); and f is the Fermi–Dirac function. The resonant levels can also be achieved by introducing impurity atoms into the $CoSb_3$-based TE material, which changes the density of states near the Fermi energy of the material and realizes the regulation of electronic transport performance.[46,47]

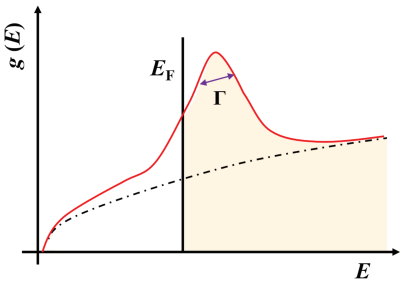


Fig. 5. Schematic representation of the density of electron states (DOS) $g(E)$ of TE semiconductors containing impurity energy levels (red line) and without impurity energy levels (dashed line). Γ is a narrow energy range, E_F is the Fermi level.

Zheng *et al.*[46] used magnetron sputtering to prepare n-type Ag/In interstitial co-doped $CoSb_3$-based TE films. According to the first principle calculation results, compared with the undoped $CoSb_3$ TE film (Fig. 6(a)), the resonance impurity level and the highest peak of DOS appear near the Fermi level for the interstitial Ag doped and Ag/In co-doped $CoSb_3$ TE film samples, which makes the electrons near the Fermi level more localized (Figs. 6(b) and 6(c)). The enhancement of DOS near the Fermi level caused by the impurity levels results in a higher S value (Fig. 6(d)). In addition, the resonant impurity levels caused by Ag and In doping make the DOS near the Fermi energy wider, resulting in the increase of electrical conductivity (Fig. 6(e)). Due to the increase in S and electrical conductivity, the power factor values of the doped samples increase significantly (Fig. 6(f)). The TE properties of doped samples are significantly higher than other TE films.[67–70] Zhao *et al.*[47] studied In-filled skutterudite TE materials through x-ray absorption fine structure spectrum, x-ray photoelectron spectroscopy, TE transport test and theoretical calculations. It was found that the electronic and thermal transport properties of materials can be regulated synergistically by the heat-carrying phonon-localized resonant scattering (Fig. 7(a)), accelerated electron movement (Fig. 7(b)) and increase in density of states near the Fermi level (Fig. 7(c)) when the In atoms are filled into Sb_{12} icosahedral void of the $CoSb_3$ material. The doping of In atoms in the $CoSb_3$ material causes resonance impurity levels, resulting in the significant increase of the density of states near the Fermi level and Seebeck coefficient (Fig. 7(d)). Therefore, it is also a very effective means to improve TE properties of the $CoSb_3$-based materials by doping to produce resonant energy levels and then increase the density of states near the Fermi level.

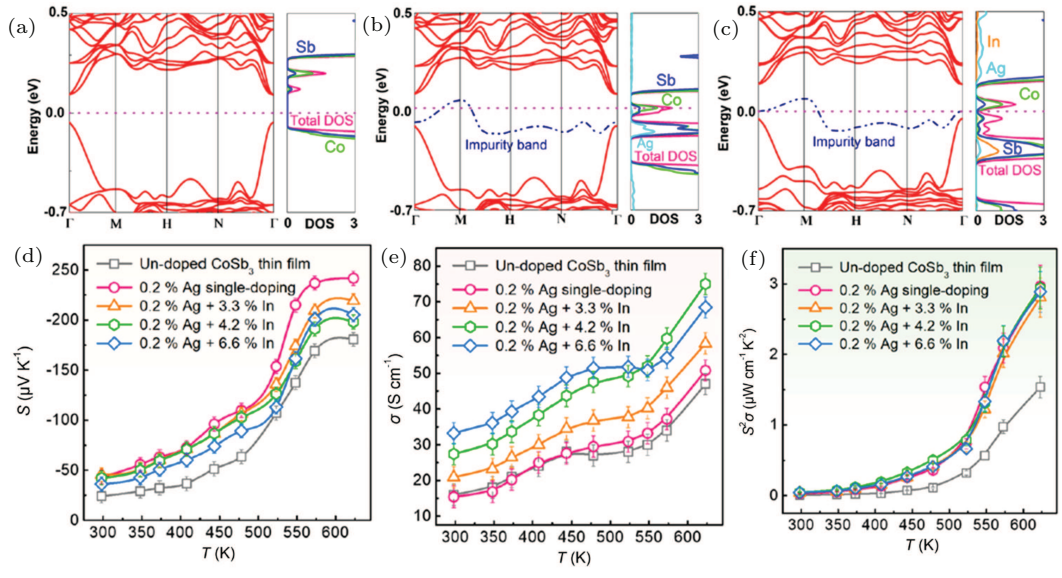


Fig. 6. Calculated band structures and DOS of (a) undoped, (b) interstitially Ag-doped and (c) interstitially Ag/In Co-doped $CoSb_3$ thin film. The temperature dependence of (d) S, (e) σ and (f) $S^2\sigma$ of as-fabricated $CoSb_3$ thin films with different Ag and In doping concentrations. Reproduced with permission from Ref. [46].

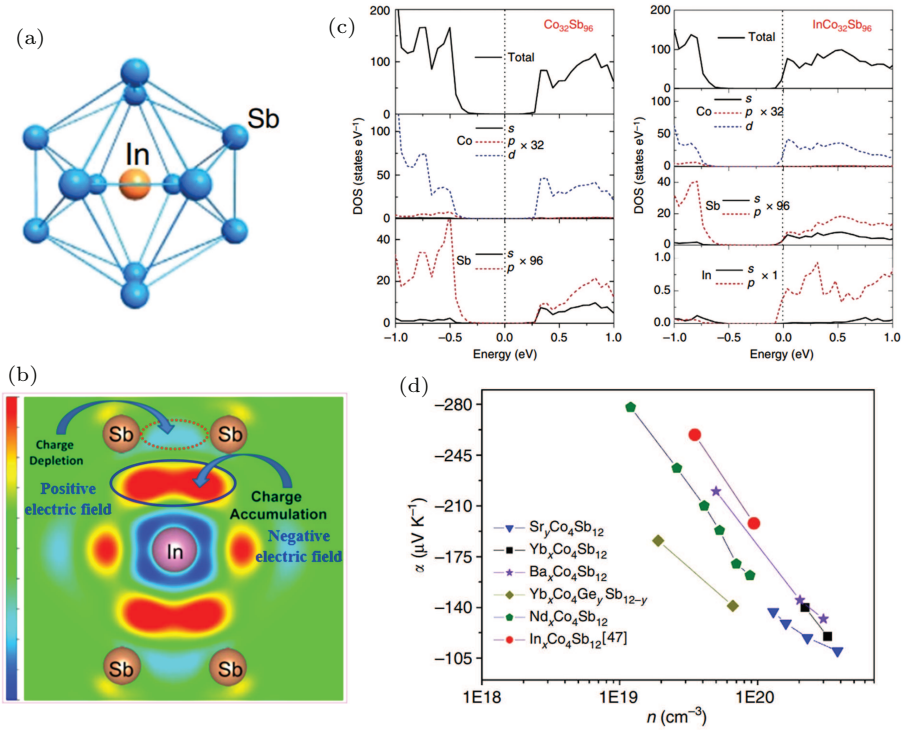


Fig. 7. (a) In atom fills Sb_{12} icosahedron voids at the 2*a* sites; (b) differential charge density of $In_{0.125}Co_4Sb_{12}$ projected on the (111) plane; (c) total DOS and partial DOS near VBM and CBM of $CoSb_3$ and $In_{0.125}Co_4Sb_{12}$; (d) Seebeck coefficient as a function of carrier concentration for n-type filled $CoSb_3$ at room temperature. Reproduced with permission from Ref. [47].

3. Charge-carrier engineering

In semiconductor TE materials, carrier concentration and mobility are two parameters closely related to the electronic transport properties of materials. The optimization of these two parameters is an important part of carrier engineering. Doping in a TE material matrix to form solid solution alloy usually affects the carrier concentration of the matrix. High performance solid solution TE materials can be obtained by optimizing the doping amount and adjusting the carrier concentration.[71,72] In addition, the carrier mobility of the matrix material can be significantly improved without reducing the carrier concentration by modulating doping,[44,48] forming a textured structure[73] or percolating carrier transports,[74] so that the matrix material can obtain higher electronic transport properties.

For $CoSb_3$-based skutterudite TE materials, the regulation of carrier concentration is usually achieved by means of element filling[17,75,76] or doping to form solid solution alloys.[77,78] Element filling usually fills alkali, alkaline earth and rare earth metals and even electronegative elements[79] into the Sb_{12} icosahedral voids of skutterudite materials to form filledskutterudite. Filling atoms are doped as donor doping. The optimal carrier concentration can be obtained by adjusting the doping amount, which further optimizes the electronic transport properties of the material. The solid solution alloy can be formed using foreign atoms to replace the framework atoms Co or Sb of the skutterudite material. The doping of foreign atoms can adjust the carrier concentration of the solid solution and improve its electronic transport performance. Recently, it is found that the introduction of magnetic nanoparticles into the $CoSb_3$-based matrix material[16,25,80] can also regulate the carrier concentration and improve the electronic transport properties of the matrix by using the magnetic phase transition of the magnetic nanoparticles. It is worth noting that the introduction of the second phase material into the $CoSb_3$-based skutterudite matrix material can significantly improve the carrier mobility of materials by using the modulated doping structures,[81–83] large grain size or low-energy grain boundaries[84] between the second phase and the matrix phase. In addition, the filling of foreign atoms can strongly scatter the heat-carrying phonons through the rattling of the filling atoms. The point defect and mass fluctuation of solid solution caused by replacement atoms can also strongly scatter the heat-carrying phonons. These changes caused by the filling and replacement of foreign atoms significantly reduce the lattice thermal conductivity. Combined with the regulation of the carrier transport characteristics of the material by the filling or doping of foreign atoms, the synergistic optimization of electronic and thermal transport properties of $CoSb_3$-based materials can be finally realized. Table 2 lists the optimized carrier concentration, mobility, and *ZT* values of some typical $CoSb_3$-based skutterudite TE materials[57,63,81–91] reported in recent years. The carrier concentration or mobility of these materials has been optimized by means of filling, doping, nanocomposite or modulation-like doping.

Table 2. The carrier concentration, carrier mobility and *ZT* value of some typical $CoSb_3$-based skutterudites TE materials optimized by the charge-carrier engineering in recent years.

Samples	n (10^{20} cm^{-3})	*ZT*	Ref.	Samples	μ (cm^2·V·s^{-1})	*ZT*	Ref.
$In_{0.3}Co_4Sb_{11.9}$	1.74	1.2	[57]	0.2wt% Ni/$Yb_{0.2}Co_4Sb_{12}$	61.3	1.07	[81]
$Ga_{0.1}Co_4Sb_{12}$	0.60	0.7	[63]	$Yb_{0.21}Co_4Sb_{12}$/0.32CoAl	40.8	1.36	[82]
0.2wt% Ni/$Yb_{0.2}Co_4Sb_{12}$	1.22	1.07	[81]	2wt% BST/$Yb_{0.2}Co_4Sb_{12}$	45	0.96	[83]
$Yb_{0.21}Co_4Sb_{12}$/0.32CoAl	3.62	1.36	[82]	$Ba_{0.15}Yb_{0.3}Co_4Sb_{14.4}$+20%Sb	48.1	1.53	[84]
$Ba_{0.15}Yb_{0.3}Co_4Sb_{14.4}$+20%Sb	3.60	1.53	[84]	Ag/$Ba_{0.3}Co_4Sb_{12}$	35.9	1.0	[88]
$Y_{0.1}Ce_{0.15}Co_4Sb_{12}$	3.75	1.18	[85]	$CoSb_{2.75}Ge_{0.05}Te_{0.2}$	19.4	1.1	[89]
$Yb_{0.26}Co_4Sb_{12}$	6.50	1.2	[86]	$Ba_{0.3}Yb_{0.3}Co_{3.6}Fe_{0.4}Sb_{12}$	16	1.35	[90]
$Fe_{0.2}Co_{3.8}Sb_{11.5}Te_{0.5}$	3.0	1.3	[87]	2%CeO+$In_{0.25}Co_4Sb_{12}$	34	1.4	[91]

3.1. Carrier concentration

There is a close correlation between the carrier concentration of TE materials and other TE physical parameters (except lattice thermal conductivity), as shown in Fig. 8. It can be seen that the TE materials can obtain a higher *ZT* value if the carrier concentration is adjusted to an appropriate value ($\sim 10^{19}$–10^{20} cm^{-3}). Shi *et al.*[17] prepared high-performance multi-filled $CoSb_3$ materials. Multifilled elements (Ba, La, Yb) were introduced into a $CoSb_3$ material, and the carrier concentration of the multifilled $CoSb_3$ material was regulated by optimizing the filling fraction of these filling atoms. The sample with the highest *ZT* value (1.7@850 K, Fig. 9(a)) corresponds to the optimized carrier concentration of 3.66×10^{20} cm^{-3}. This carrier concentration is located in the high power factor region (Fig. 9(b)). Furthermore, the sample with the optimal carrier concentration can scatter broadband phonons due to the rattling of the multi-filled atoms in the Sb_{12} icosahedral void of $CoSb_3$, resulting in the lowest thermal conductivity (Fig. 9(c)). Therefore, this sample has the highest TE transport properties (Fig. 9(a)). Anno *et al.*[77] studied the effect of partial substitution of Co with different elements *M* (*M* = Ni, Pd, Pt and Pd+Pt) on the TE properties of $CoSb_3$ materials ($Co_{1-x}M_xSb_3$). The carrier concentration of the solid solution can be regulated by optimizing the doping amount of M element (Fig. 9(d)), and then a high-performance $Co_{1-x}M_xSb_3$ solid solution TE material can be obtained.

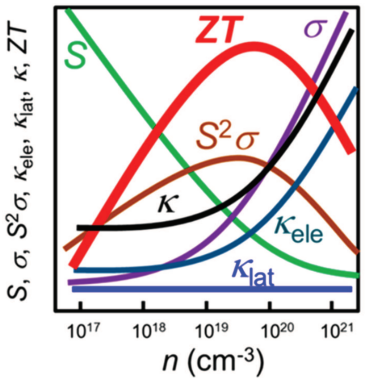


Fig. 8. *ZT* and its related parameters as a function of carrier concentration. Reproduced with permission from Ref. [48].

Zhao *et al.*[25] prepared magnetic nanocomposite TE materials by introducing $BaFe_{12}O_{19}$ hard magnetic nanoparticles (BaM-NPs) into n-type (Ba, In) double-filled $CoSb_3$ matrix materials. BaM-NPs in the ferromagnetic state can capture electrons of matrix due to its strong micro-magnetic field when the working temperature of the magnetic nanocomposite materials is lower than the Curie temperature of BaM-NPs, which only reduces the carrier concentration (Fig. 10(a)). There is no abnormality in the relationship between the electrical conductivity/Seebeck coefficient of the composite material and the temperature. When the working temperature exceeds the Curie temperature, BaM-NPs in the paramagnetic state release trapped electrons because of the disappearance of the micro-magnetic field, resulting in the significant increase of carrier concentration (Fig. 10(a)). The electrical conductivity and the Seebeck coefficient of the composite exhibited anomalous transport phenomena different from those of the matrix (Figs. 10(b) and 10(c)). BaM-NPs play the role of an "electron repository" before and after the ferromagnetic-paramagnetic transition. When the curie temperature of BaM-NPs is close to the intrinsic excitation temperature ($\sim$ 675 K) of the filled $CoSb_3$ matrix, the "electron repository" effect of the magnetic nanoparticles in the ferromagnetic-to-paramagnetic transition can effectively regulate the carrier concentration and inhibit the deterioration of TE performance under intrinsic excitation of the matrix (Fig. 10(d)). Our research group[80] also introduced BaM-NPs into an In single-filled $CoSb_3$ matrix material and used its electron repository effect to regulate the carrier concentration of the $In_{0.25}Co_4Sb_{12}$ matrix material (Fig. 10(e)). The purpose of suppressing the performance degradation of the intrinsic excitation region for the filled $CoSb_3$ material is also achieved (Fig. 10(f)). Zhao *et al.*[16] also introduced soft magnetic Co (Fe or Ni) nanoparticles into the (Ba, In) double-filled $CoSb_3$ matrix (Fig. 10(g)). Using the different work function between the soft magnetic metal nanoparticles and the skutterudite semiconductor material, the transfer of electrons from Co nanoparticles to skutterudite semiconductor is realized (Fig. 10(h)), which regulates the carrier concentration of the matrix and significantly improves the electrical conductivity of magnetic nanocomposites (Fig. 10(i)). Therefore, forming solid solution by doping, filling or introducing magnetic nano second phase is an effective means to optimize the carrier concentration of $CoSb_3$-based materials and further to improve their TE properties.

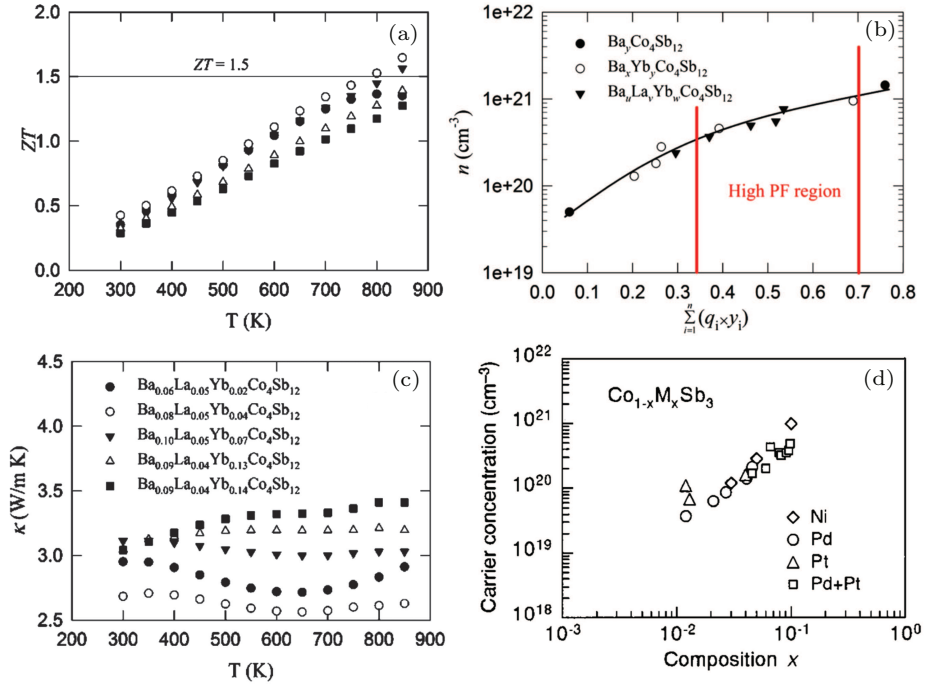


Fig. 9. (a) Temperature dependence of ZT for $Ba_uLa_vYb_wCo_4Sb_{12}$ multi-filled skutterudites; (b) carrier concentration as a function of $(\sum_{i=1}^{n} q_i \times y_i)$ for partially filled $CoSb_3$, where q_i is the effective charge state and y_i is the filling fraction of the ith filler in multiple-filled skutterudites. The red lines enclose the estimated high power factor region; (c) temperature dependence of total thermal conductivity for $Ba_uLa_vYb_wCo_4Sb_{12}$ multi-filled skutterudites. Reproduced with permission from Ref. [17]. (d) Hall carrier concentration at room temperature as a function of composition x for $Co_{1-x}M_xSb_3$ (M = Ni, Pd, Pt and Pd+Pt) samples. Reproduced with permission from Ref. [77].

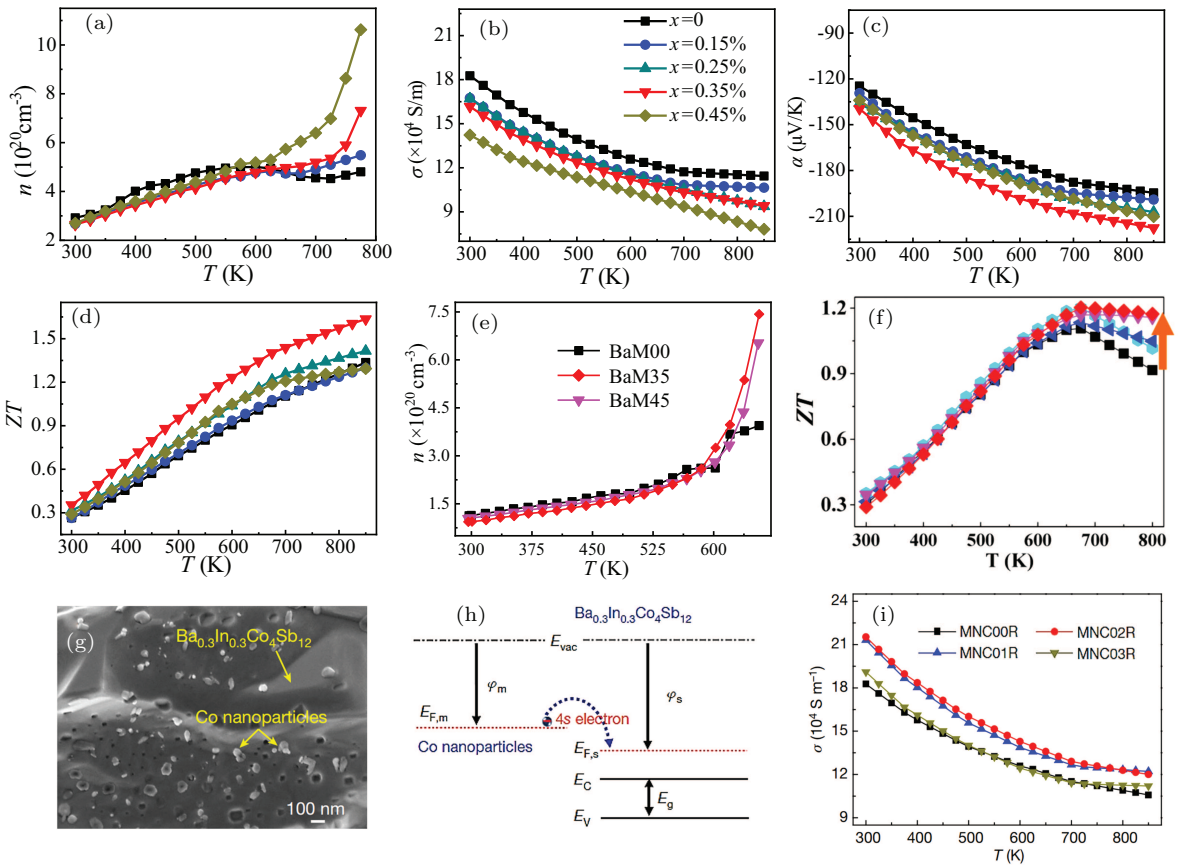


Fig. 10. Temperature dependence of (a) carrier concentration n, (b) electric conductivity σ, (c) Seebeck coefficient α and (d) ZT values of xBaFe$_{12}$O$_{19}$/$Ba_{0.3}In_{0.3}Co_4Sb_{12}$ materials. Reproduced with permission from Ref. [25]. Temperature dependence of (e) carrier concentration n and (f) ZT values of $In_{0.25}Co_4Sb_{12}$ matrix (BaM00) and xBaFe$_{12}$O$_{19}$/$In_{0.25}Co_4Sb_{12}$ nanocomposites (BaM15, BaM25, BaM35 and BaM45). Reproduced with permission from Ref. [80]. (g) Field emission scanning electron microscopy (FESEM) image of the xCo/$Ba_{0.3}In_{0.3}Co_4Sb_{12}$ sample with $x = 0.2\%$ (MNC02R); (h) schematic of the charge transfer of 4s electrons from the Co nanoparticles to the matrix; φ_m and φ_s are the work functions of the Co nanoparticles and the matrix, respectively; (i) temperature dependence of electric conductivity σ of xCo/$Ba_{0.3}In_{0.3}Co_4Sb_{12}$ samples (MNC00R, MNC01R, MNC02R and MNC03R). Reproduced with permission from Ref. [16].

3.2. Carrier mobility

Filling and alloying are an important means to regulate the carrier concentration of $CoSb_3$-based skutterudite materials. Filled and alloyed $CoSb_3$-based skutterudite materials are generally heavily doped semiconductors, and their carrier concentrations are mostly in the range of 10^{19}–10^{21} cm^{-3}. High concentration of ionized impurity scattering in heavily doped semiconductor materials is unfavorable to the improvement of carrier mobility.[92] In order to weaken ionized impurity scattering and to obtain higher carrier mobility, the concept of modulated doping[93] have been proposed. This method is mostly used in thin-film materials.[94] For bulk materials, the heavily doped second phase can be locally embedded in the matrix phase to form the modulation structure. Combined with energy band modification, carriers of heavily doped region are spatially separated from the matrix atoms and can move freely into undoped particles (Figs. 11(a) and 11(c)).[48] Therefore, the modulation doping will reduce the effect of ionized impurities on the carriers compared with conventional uniformly doping, resulting in a significant increase of the carrier mobility.[43]

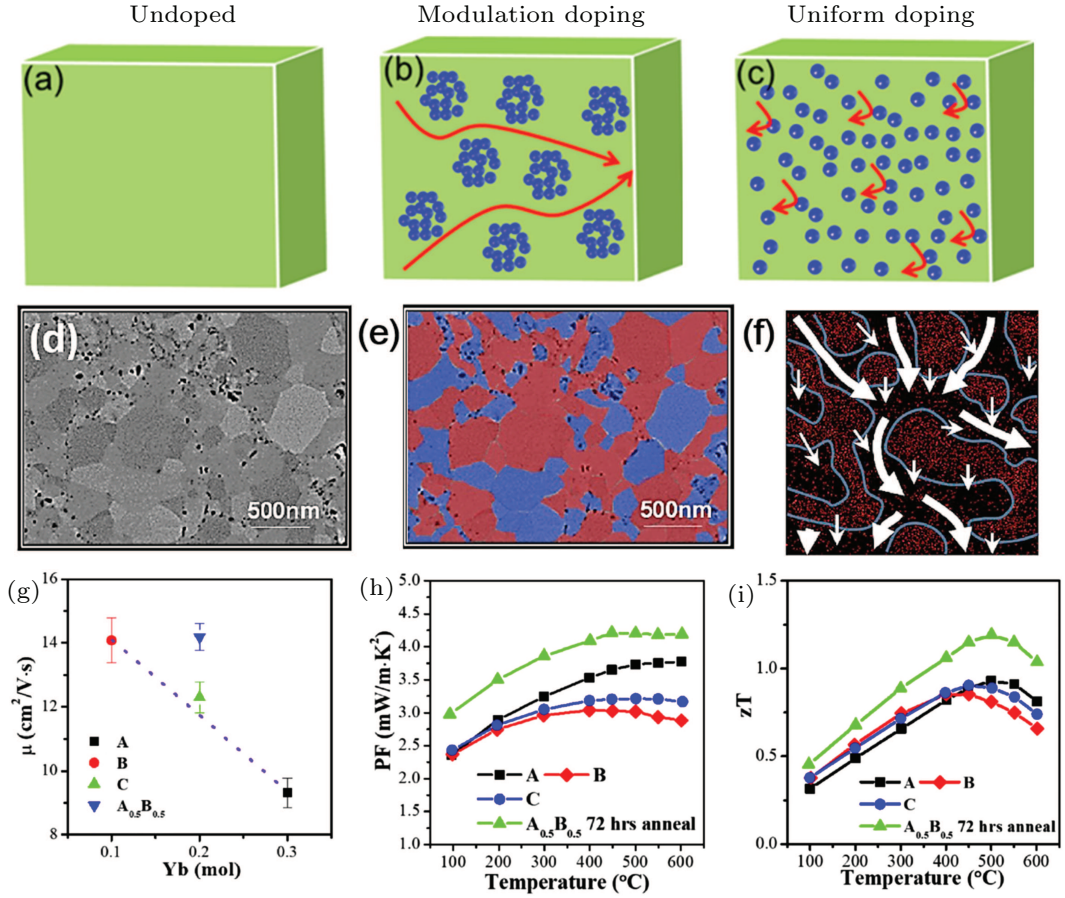


Fig. 11. Schematic representation of (a) nondoped semiconductor, (b) schematic representation of modulation doping, where two types of grains consisting of nondoped and heavily doped semiconductors are spatially separated and (c) schematic representation of uniform doped semiconductor, where dopants are uniformly dispersed in the host matrix. Reproduced with permission from Ref. [48]. (d) BSE image of an $A_{0.5}B_{0.5}$ sample showing nano-crystalline grains; (e) colors (red: Yb-rich grain-$A_{0.5}$; blue: Yb-deficient grain-$B_{0.5}$) highlight the features of BHJ structure; (f) schematic picture showing carriers transmission in the $A_{0.5}B_{0.5}$ sample; (g) room-temperature Hall carrier mobility (μ_H) as function of Yb content for the A, B, C and $A_{0.5}B_{0.5}$ samples; Temperature dependences of (h) power factor (PF) and (i) *ZT* values for A, B, $A_{0.5}B_{0.5}$ and C samples. Reproduced with permission from Ref. [49].

Nie *et al.*[49] successfully prepared an n-type filled skutterudite bulk material with a heterojunction (BHJ) structure. This material with the BHJ structure is composed of two n-type filled skutterudite materials (A: $Yb_{0.3}Ca_{0.1}Al_{0.1}Ga_{0.1}In_{0.1}Fe_{0.25}Co_{3.75}Sb_{12}$; B: $Yb_{0.1}Ca_{0.1}Al_{0.1}Ga_{0.1}In_{0.1}Fe_{0.25}Co_{3.75}Sb_{12}$) with different Yb filling fractions. This BHJ material (labeled $A_{0.5}B_{0.5}$) with rich nanostructures was prepared by mixing and annealing two Yb filled skutterudites for A and B volume ratio of 1:1 (Figs. 11(d) and 11(e)). For comparison, C material with nominal composition of $Yb_{0.2}Ca_{0.1}Al_{0.1}Ga_{0.1}In_{0.1}Fe_{0.25}Co_{3.75}Sb_{12}$ was also prepared. C material and $A_{0.5}B_{0.5}$ material have similar carrier concentrations due to the similar Yb filling fraction. The structure of the $A_{0.5}B_{0.5}$ sample is similar to the modulated doping structure in Fig. 11(b), as shown in Fig. 11(f). The C material structure is similar to the uniformly doped structure of Fig. 11(c). Under the same carrier concentration, the carrier mobility of

the $A_{0.5}B_{0.5}$ sample is significantly higher than that of the C sample (Fig. 11(g)), which is attributed to the modulated doping structure of the $A_{0.5}B_{0.5}$ sample. In this BHJ structure, the dark red region has a higher carrier concentration, and the light red region has low carrier concentration, forming a concentration gradient. In order to achieve equilibrium, the carriers will be rapidly transported from the dark red region to the light red region (Fig. 11(f)), which greatly improves the mobility of the $A_{0.5}B_{0.5}$ material. Due to its rich nanostructure and high mobility, the $A_{0.5}B_{0.5}$ sample has high electronic transport properties (Fig. 11(h)) and low lattice thermal conductivity. Therefore, compared with other samples (A, B and C), the $A_{0.5}B_{0.5}$ sample has the best TE properties (Fig. 11(i)). Fu *et al.*[81] prepared Ni-doped $Yb_{0.2}Co_4Sb_{12}$ skutterudite with a special "core-shell" microstructure. The difference in Ni contents between the special core-shell nanograins and the skutterudite matrix grains also forms a similarly modulated doping structure. Ni replaces the Co sites of skutterudite in the core-shell nanograins, so that the core-shell structure has a high carrier concentration, while the matrix grains have a lower carrier concentration. Therefore, a carrier concentration gradient is generated in Ni-doped $Yb_{0.2}Co_4Sb_{12}$ skutterudite. In order to achieve equilibrium, the carriers are rapidly transported from the core-shell nanograins to the normal matrix grains, which greatly improve the mobility of the material (matrix sample: 23.44 $cm^2 \cdot V^{-1} \cdot S^{-1}$, 0.2 wt% Ni/$Yb_{0.2}Co_4Sb_{12}$ sample: 53.17 $cm^2 \cdot V^{-1} \cdot S^{-1}$). Peng *et al.*[83] also prepared $Yb_{0.2}Co_4Sb_{12}$-$Bi_{0.4}Sb_{1.6}Te_3$ nanocomposites with similar modulation doping structure. Compared with the $Yb_{0.2}Co_4Sb_{12}$ matrix material, the composite material has higher carrier mobility. This is mainly due to the fact that the $Bi_{0.4}Sb_{1.6}Te_3$ material with high mobility in the composite material is dispersed in the matrix with low mobility to form a structure similar to that of modulation doping.

In addition, the structure of large grain size and low energy grain boundaries can also significantly improve the carrier mobility of the material. Qin *et al.*[84] successfully prepared (Ba, Yb) double-filled $CoSb_3$ materials with excessive Sb by liquid-phase compaction method. Under the same carrier concentration, the carrier mobility of the $Ba_xYb_{0.3}Co_4Sb_{12}$+20%Sb sample is significantly higher than other reported double-filled or multi-filled skutterudite materials.[75,95–97] The excellent carrier mobility is mainly attributed to two aspects: On the one hand, the samples prepared by liquid phase compaction method have large grains. According to the Ostwald ripening theory,[98] larger grains tend to gobble up smaller grains, which will accelerate the transport of carriers. On the other hand, low-energy grain boundaries with dense dislocation arrays have no negative effect on electron transport, even positive effects. This has also been reported in other material systems.[99–101] Therefore, it is an effective method to increase the carrier mobility of $CoSb_3$-based materials by forming modulation doped structures or preparing the structures with large grains and low-energy grain boundaries.

4. Summary and perspectives

This review summarizes some main research progresses in recent years to optimize the TE transport properties of $CoSb_3$-based materials through energy band and charge-carrier engineering. The Seebeck coefficient of $CoSb_3$-based materials was significantly improved by the band engineering of band convergence and resonance levels induced by doping and/or filling. Combined with the strong phonon scattering caused by doping and/or filling, the thermal and electronic transport parameters are decoupled, which greatly improves the TE properties of $CoSb_3$-based materials. In addition, the electronic transport properties of $CoSb_3$-based materials were significantly improved by the charge-carrier engineering with the increase of carrier concentration or mobility. The optimization of carrier concentration can be obtained by forming solid solution by doping, filling or introducing magnetic nano second phase. The increase of carrier mobility can be obtained by forming modulation doped structures or preparing the structures with large grains and low-energy grain boundaries. Combined with the strong phonon scattering caused by doping, filling, or the introduction of the nano-interface, the thermal and electronic transport parameters are also decoupled, which greatly improves the TE properties of $CoSb_3$-based materials. However, there are still some problems in research of energy band and charge-carrier engineering of $CoSb_3$-based skutterudite TE materials, which need to be further studied: (i) It is very important to further develop new processes to prepare materials with high carrier mobility and new modulated doping structures. (ii) On the basis of theory and experiment, further screening of appropriate doping/filling elements and nano second phase can make the energy band of $CoSb_3$ based TE materials converge significantly or produce obvious resonance energy level. This is the key to improve the transport properties of $CoSb_3$ based TE materials again. It should be noted that the screened nano second phase should have appropriate energy band matching with the $CoSb_3$ based matrix at the phase interface and have stable physical and chemical properties. (iii) Further screening of appropriate doping/filling elements and nano second phase makes the carrier concentration of $CoSb_3$ based materials appear in the optimal concentration range (10^{19} cm^{-3}–10^{20} cm^{-3}) and have high carrier mobility. This is the key to improve the TE transport performance of $CoSb_3$ based materials again.

In conclusion, plenty of work remains to be carried out to further improve the TE transport properties of $CoSb_3$-based TE materials through energy band and charge-carrier engineering. Though the challenges are pervasive, the research ac-

tivities of TE materials are still hot all over the world. The field of TE materials attracts more and more researchers. Interdisciplinary exchanges between physicists, chemists, mathematicians, material scientists and device engineers are also deepening. The interdisciplinary research of TE materials and other disciplines are becoming more and more extensive, which will promote the sustained and rapid growth of TE research and future large-scale applications.

Acknowledgements

This review was supported by the National Natural Science Foundation of China (Grant No. 51872006) and the Excellent Youth Project of Natural Science Foundation of Anhui Province of China (Grant No. 2208085Y17).

References

[1] Bell L E 2008 *Science* **321** 1457
[2] Snyder G J and Toberer E S 2011 *Nat. Mater.* **7** 105
[3] Biswas K, He J Q, Blum I D, Wu C I, Hogan T P, Seidman D N, Dravid V P and Kanatzidis M G 2012 *Nature* **489** 414
[4] Xiao Y, Wu H J, Li W, Yin M J, Pei Y L, Zhang Y, Fu L W, Chen Y X, Pennycook S J, Huang L, He J Q and Zhao L D 2017 *J. Am. Chem. Soc.* **139** 18732
[5] Moshwan R, Yang L, Zou J and Chen Z G 2017 *Adv. Funct. Mater.* **27** 1703278
[6] Sui J, Li J, He J, Pei Y L, Berardan D, Wu H, Dragoe N, Cai W and Zhao L D 2013 *Energ. Environ. Sci.* **6** 2916
[7] Xia K Y, Hu C, Fu C L, Zhao X B and Zhu T J 2021 *Appl. Phys. Lett.* **118** 140503
[8] Sales B C, Mandrus D and Williams R K 1996 *Science* **272** 1325
[9] Zhao W Y, Liang Z, Wei P, Yu J, Zhang Q J and Shao G S 2012 *Acta Mater.* **60** 1741
[10] Yang D W, Su X L, He J, Yan Y G, Li J, Bai H, Luo T T, Liu Y M, Luo H, Yu Y M, Wu J S, Zhang Q J, Uher C and Tang X F 2021 *Nat. Commun.* **12** 6077
[11] Zong P A, Hanus R, Dylla M, Tang Y S, Liao J C, Zhang Q H, Snyder G and Chen L 2017 *Energy Environ. Sci.* **10** 183
[12] Jing H M, Tong X, Zhu J L, Yang T, Xia A L, Liu Z Y and Jin C G 2021 *Ceram. Int.* **47** 24916
[13] Zhu J L, Tong X, Niu S, Liu Z Y and Xu D 2021 *J. Wuhan Univ. Technol.* **36** 353
[14] Tong X, Liu Z Y, Zhu J L, Yang T, Wang Y G and Xia A L 2021 *Front. Mater. Sci.* **15** 317
[15] Liu Z Y, Zhu W T, Nie X L and Zhao W Y 2019 *J. Mater. Sci.-Mater. El.* **30** 12493
[16] Zhao W Y, Liu Z Y, Sun Z G, Zhang Q J, Wei P, Mu X, Zhou H Y, Li C C, Ma S F, He D Q, Ji P X, Zhu W T, Nie X L, Su X L, Tang X F, Shen B G, Dong X L, Yang J H, Liu Y and Shi J 2017 *Nature* **549** 247
[17] Shi X, Yang J, Salvador J R, Chi M F, Cho J, Wang H, Bai S Q, Yang J H, Zhang W Q and Chen L D 2011 *J. Am. Chem. Soc.* **133** 7837
[18] Rogl G, Bursik J, Grytsiv A, Puchegger S, Soprunyuk V, Schranz W, Yan X, Bauer E and Roo R 2018 *Acta. Mater.* **145** 359
[19] Saeed M, Khan B, Ahmad I, Saleemi A S, Rehman N, Aliabad H A R and Uddin S 2019 *RSC. Adv.* **9** 24981
[20] Cailiat T, Borshchevsky A and Fleurial J P 1996 *J. Appl. Phys.* **80** 4442
[21] Liu Z Y, Zhu J L, Tong X, Niu S and Zhao W Y 2020 *J. Adv. Ceram.* **9** 647
[22] Toprak M S, Stiewe C, Platzek D, Williams S, Bertini L, Müller E, Gatti C, Zhang Y, Rowe M and Muhammed M 2004 *Adv. Funct. Mater.* **14** 1189
[23] Mi J L, Zhu T J and Zhao X B 2007 *J. Appl. Phys.* **101** 054314
[24] Ahmed A and Han S 2019 *J. Alloys. Compd.* **790** 577
[25] Zhao W Y, Liu Z Y, Wei P, Zhang Q J, Zhu W T, Su X L, Tang X F, Yang J H, Liu Y, Shi J, Chao Y M, Lin S Q and Pei Y Z 2017 *Nat. Nanotechnol.* **12** 55
[26] Qin D D, Wu H J, Cai S T, Zhu J B, Cui B, Yin L, Qin H X, Shi W J, Zhang Y, Zhang Q, Liu W S, Cao J, Pennycook S J, Cai W and Sui J H 2019 *Adv. Energy Mater.* **9** 1902435
[27] Ghosh S, Shankar G, Karati A, Rogl G, Rogl P, Bauer E, Murty B S, Suwas S and Mallik R C 2020 *Dalton Trans.* **49** 15883
[28] Zhu J L, Liu Z Y, Tong X, Xia A L, Xu D, Lei Y, Yu J, Tang D G, Ruan X F and Zhao W Y 2021 *ACS Appl. Mater. Interfaces* **13** 23894
[29] Yu J, Zhao W Y, Wei P, Zhu W, Zhou H Y, Liu Z Y, Tang D G, Lei B and Zhang Q J 2014 *Appl. Phys. Lett.* **104** 142104
[30] Khan A U, Kobayashi K, Tang D M, Yamauchi Y, Hasegawa K, Mitome M, Xue Y, Jiang B Z, Tsuchiya K, Golberg D, Bando Y and Mori T 2017 *Nano Energy* **31** 152
[31] Yang H J, Wen P F, Zhou X L, Li Y, Duan B, Zhai P C and Zhang Q J 2019 *Scripta Mater.* **159** 68
[32] Xi L L, Yang J, Shi X, Zhang W Q, Chen L D and Yang J H 2011 *Sci. Sin.-Phys. Mech. Astron.* **41** 706
[33] Shi X, Kong H, Li C P, Uher C, Yang J, Salvador J R, Wang H, Chen L and Zhang W 2008 *Appl. Phys. Lett.* **92** 182101
[34] Guo S P, Anand S, Brod M K, Zhang Y S and Snyder G J 2022 *J. Mater. Chem. A* **10** 3051
[35] Liu W, Tan X J, Yin K, Liu H J, Tang X F, Shi J, Zhang Q J and Uher C 2012 *Phys. Rev. Lett.* **108** 166601
[36] Pei Y Z, Shi X Y, LaLonde A, Wang H, Chen L D and Snyder G J 2011 *Nature* **473** 66
[37] Qin B C, Wang D Y, Liu X X, Qin Y X, Dong J F, Luo J F, Li J W, Liu W, Tan G J, Tang X, Li J F, He J Q and Zhao L D 2021 *Science* **373** 556
[38] Xu W J, Zhang Z W, Liu C Y, Ga J, Ye Z Y, Chen C G, Peng Y, Bai X B and Miao L 2021 *J. Adv. Ceram.* **10** 860
[39] Valiyaveettil S M, Nguyen D L, Wong D P, Hsing C R, Paradis-Fortin L, Qorbani M, Sabbah A, Chou T L, Wu K K, Rathinam V, Wei C M, Chen L C and Chen K H 2022 *Inorg. Chem.* **61** 4442
[40] Chen Z Y, Guo X M, Zhang F J, Shi Q, Tang M J and Ang R 2020 *J. Mater. Chem. A* **8** 16790
[41] Ibáñez M, Hasler R, Genç A, Liu Y, Kuster B, Schuster M, Dobrozhan O, Cadavid D, Arbiol J, Cabot A and Kovalenko M V 2019 *J. Am. Chem. Soc.* **141** 8025
[42] Xu F, Zhang D, Gao S K, Yang L, San X Y, Li Z L, Qian X, Yang J Y and Wang S F 2022 *Scripta Mater.* **208** 114360
[43] Zhao L D, Wang S and Xiao Y 2021 *Acta Metall. Sin.* **57** 1171 (in Chinese)
[44] Pei Y L, Wu H, Wu D, Zheng F and He J 2014 *J. Am. Chem. Soc.* **136** 13902
[45] Wang Z Y, Xi J Y, Ning J Y, Guo K, Duan B, Luo J, Snyder G J, Yang J and Zhang W Q 2021 *Chem. Mater.* **33** 1046
[46] Zheng Z H, Shi X L, Ao D W, Liu W D, Chen Y X, Li F, Chen S, Tian X Q, Li X R, Duan J Y, Ma H L, Zhang X H, Liang G X, Fan P and Chen Z G 2021 *Nano Energy* **81** 105683
[47] Zhao W Y, Wei P, Zhang Q J, Peng H, Zhu W T, Tang D G, Yu J, Zhou H Y, Liu Z Y, Mu X, He D Q, Li J C, Wang C L, Tang X F and Yang J H 2015 *Nat. Commun.* **6** 6197
[48] Tan G J, Zhao L D and Kanatzidis M G 2016 *Chem. Rev.* **116** 12123
[49] Nie G, Li W J, Guo J Q, Yamamoto A, Kimura K, Zhang X M, Isaacs E B, Dravid V, Wolverton C, Kanatzidis M G and Priya S 2019 *Nano Energy* **66** 104193
[50] Zhu T J, Liu Y T, Fu C G, Heremans J P, Snyder J G and Zhao X B 2017 *Adv. Mater.* **29** 1605884
[51] Cutler M, Leavy J F and Fitzpatrick R L 1964 *Phys. Rev.* **133** A1143
[52] Heremans J P, Wiendlocha B and Chamoire A M 2012 *Energy Environ. Sci.* **5** 5510
[53] Zhang Q Y, Wang H, Liu W S, Wang H Z, Yu B, Zhang Q, Tian Z Y, Ni G, Lee S. Esfarjani K, Chen G and Ren Z F 2012 *Energy Environ. Sci.* **5** 5246
[54] Liu, H T, Sun Q, Zhong Y, Xia, C L, Chen Y, Chen Z G and Ang R 2022 *Chem. Eng. J.* **428** 132601
[55] Koenig J D, Nielsen M D, Gao Y B, Winkler M, Jacquot A, Bottner H and Heremans J P 2011 *Phys. Rev. B* **84** 205126

[56] Leszczynski J, Ros V, Lenoir B, Dauscher A, Candolfi C, Masschelein P, Hejtmanek J, Kutorasinski K, Tobola J, Smith R I, Stiewe C and Muller E 2013 *J. Phys. D: Appl. Phys.* **46** 495106

[57] Tang Y L, Qiu Y T, Xi L L, Shi X, Zhang W Q, Chen L D, Tseng S M, Chen S W and Snyder G J 2014 *Energy Environ. Sci.* **7** 812

[58] Tu Z K, Sun X, Li X, Li R X, Xi L L and Yang J 2019 *Aip. Adv.* **9** 045325

[59] Tang Y L, Gibbs Z M, Agapito L A, Li G D, Kim H S, Nardelli M B, Curtarolo S and Snyder G J 2015 *Nat. Mater.* **14** 1223

[60] Hanus R, Guo X Y, Tang Y L, Li G D, Snyder G J and Zeier W G 2017 *Chem. Mater.* **29** 1156

[61] Shi X Y, Yang J, Wu L J, Salvador J R, Zhang C, Villaire W L, Haddad D, Yang J H, Zhu Y M and Li Q 2015 *Sci. Rep.* **5** 14641

[62] Zhang J L, Zhang L X, Ren W Q, Gou W Q, Zhang J C and Geng H Y 2021 *ACS Appl. Mater. Interfaces* **13** 29809

[63] Qiu Y T, Xi L L, Shi X, Qiu P F, Zhang W Q, Chen L D, Salvador J R, Cho J Y, Yang J H, Chien Y C, Chen S W, Tang Y L and Snyder G J 2013 *Adv. Funct. Mater.* **23** 3194

[64] Bhardwaj R, Raghuvanshi P R, Dhakate S R, Bathula S, Bhattacharya A and Gahtori B 2021 *ACS Appl. Energy Mater.* **4** 14210

[65] Koleżyński A and Szczypka W 2017 *J. Alloys Compod.* **691** 299

[66] Cutler M and Mott N F 1969 *Phys. Rev.* **181** 1336

[67] Kumar S R S, Barasheed A Z and Alshareef H N 2013 *ACS Appl. Mater. Interfaces* **5** 7268

[68] Varghese T, Hollar C, Richardson J, Kempf N, Han C, Gamarachchi P, Estrada D, Mehta R J and Zhang Y L 2016 *Sci. Rep.* **6** 33135

[69] Wan C L, Gu X K, Dang F, Itoh T, Wang Y F, Sasaki H, Kondo M, Koga K, Yabuki K, Snyder G J, Yang R J and Koumoto K 2015 *Nat. Mater.* **14** 622

[70] Fu G S, Zuo L, Chen J, Lu M and Yu L Y 2015 *J. Appl. Phys.* **117** 125304

[71] Zhong Y, Tang J, Liu H T, Chen Z W, Lin L W, Ren D, Liu B and Ang R 2020 *ACS Appl. Mater. Interfaces* **12** 49323

[72] Liu H T, Sun Q, Zhong Y, Deng Q, Gan L, Lv F L, Shi X L, Chen Z G and Ang R 2022 *Nano Energy* **91** 106706

[73] Zhu T J, Xu Z J, He J, Shen J J, Zhu S, Hu L P, Tritt T M and Zhao X B 2013 *J. Mater. Chem. A* **1** 11589

[74] Wang S N, Xiao Y, Ren D D, Su L Z, Qiu Y T and Zhao L D 2020 *J. Alloy. Compd.* **836** 155473

[75] Zhao W Y, Wei P, Zhang Q J, Dong C L, Liu L S and Tang X F 2009 *J. Am. Chem. Soc.* **131** 3713

[76] Rogl G, Grytsiv A, Rogl P, Peranio N, Bauer E, Zehetbauer M and Eibl O 2014 *Acta Mater.* **63** 30

[77] Anno H and Matsubara K 1999 *J. Appl. Phys.* **86** 3780

[78] Su X L, Li H, Yan Y G, Wang G Y, Chi H, Zhou X Y, Tang X F, Zhang Q J and Uher C 2012 *Acta Mater.* **60** 3536

[79] Duan B, Yang J, Salvador J R, He Y, Zhao B, Wang S Y, Wei P, Ohuchi F S, Zhang W Q, Hermann R P, Gourdon O, Mao S X, Cheng Y W, Wang C M, Liu J, Zhai P C, Tang X F, Zhang Q J and Yang J H 2016 *Energy Environ. Sci.* **9** 2090

[80] Liu Z Y, Zhu J L, Wei P, Zhu W T, Zhao W Y, Xia A L, Xu D, Lei Y and Yu J 2019 *ACS Appl. Mater. Interfaces* **11** 45875

[81] Fu L W, Yang J Y, Peng J Y, Jiang Q H, Xiao Y, Luo Y B, Zhang D, Zhou Z W, Zhang M Y, Cheng Y D and Cheng F Q 2015 *J. Mater. Chem. A* **3** 1010

[82] Qin D D, Cui B, Zhu J B, Shi W J, Qin H X, Guo F K, Cao J, Cai W and Sui J H 2020 *ACS Appl. Mater. Interfaces* **12** 12930

[83] Peng J Y, Zheng J, Shen F H, Zhang K, He J, Zeng J S, Xiao W L and An B 2016 *Intermetallics* **76** 33

[84] Qin D D, Cui B, Meng X F, Qin P, Xie L, Zhang Q, Liu W S, Cao J, Cai W and Sui J H 2019 *Mater. Today Phys.* **8** 128

[85] Qin D D, Shi W J, Xue W, Qin H X, Cao J, Cai W, Wang Y and Sui J H 2020 *Mater. Today Phys.* **13** 100206

[86] Li Y, Qiu P F, Xiong Z, Chen J K, Nunna R, Shi X and Chen L D 2015 *Aip Adv.* **5** 117239

[87] Mallik R C, Anbalagan R, Rogl G, Royanian E, Heinrich P, Bauer E, Rogl P and Suwas S 2013 *Acta Mater.* **61** 6698

[88] Zhou X Y, Wang G Y, Zhang L, Chi H, Su X L, Sakamoto J and Uher C 2012 *J. Mater. Chem.* **22** 2958

[89] Su X L, Li H, Wang G Y, Chi H, Zhou X Y, Tang X F, Zhang Q J and Uher C 2011 *Chem. Mater.* **23** 2948

[90] Ballikaya S and Uher C 2014 *J. Alloys. Compd.* **585** 168

[91] Benyahia M, Ohorodniichuk V, Leroy E, Dauscher A, Lenoir B and Alleno E 2018 *J. Alloys. Compd.* **735** 1096

[92] Zhang X Y and Pei Y Z 2017 *Npj Quantum Mater.* **2** 68

[93] Zebarjadi M, Joshi G, Zhu G H, Yu B, Minnich A, Lan Y C, Wang X W, Dresselhaus M, Ren Z F and Chen G 2011 *Nano Lett.* **11** 2225

[94] Tsukazaki A, Akasaka S, Nakahara K, Ohno Y, Ohno H, Maryenko D, Ohtomo A and Kawasaki M 2010 *Nat. Mater.* **9** 889

[95] Salvador J R, Waldo R A and Wong C A 2013 *Mater. Sci. Eng. B* **178** 1087

[96] Shi X, Kong H, Li C P, Uher C, Yang J, Salvador J R, Wang H, Chen L and Zhang W 2008 *Appl. Phys. Lett.* **92** 182101

[97] Bai S Q, Pei Y Z, Chen L D, Zhang W Q, Zhao X Y and Yang J 2009 *Acta Mater.* **57** 3135

[98] Kim Y J, Zhao L D, Kanatzidis M G and Seidman D N 2017 *ACS Appl. Mater. Interfaces* **9** 21791

[99] Kim S I, Lee K H, Mun H A, Kim H S, Hwang S W, Roh J W, Yang D J, Shin W H, Li X S, Lee Y H, Snyder G J and Kim S W 2015 *Science* **348** 109

[100] Meng X F, Liu Z H, Cui B, Qin D D, Geng H Y, Cai W, Fu L W, He J Q, Ren Z F and Sui J H 2017 *Adv. Energy Mater.* **7** 1602582

[101] Hwang J Y, Kim J, Kim H S, Kim S I, Lee K H and Kim S W 2018 *Adv. Energy Mater.* **8** 1800065